International Journal of Solids and Structures 50 (2013) 2817–2828

Contents lists available at SciVerse ScienceDirect

International Journal of Solids and Structures

journal homepage: www.elsevier.com/locate/ijsolstr

Effective spring stiffness for a periodic array of interacting coplanar penny-shaped cracks at an interface between two dissimilar isotropic materials

Huseyin Lekesiz [a,1], Noriko Katsube [a,*], Stanislav I. Rokhlin [b], Robert R. Seghi [c]

[a] Department of Mechanical Engineering, The Ohio State University, Columbus, OH, USA
[b] Department of Materials Science and Engineering, The Ohio State University, Columbus, OH, USA
[c] College of Dentistry, The Ohio State University, Columbus, OH, USA

ARTICLE INFO

Article history:
Received 30 August 2012
Received in revised form 21 January 2013
Available online 11 May 2013

Keywords:
Penny-shaped cracks
Dissimilar materials
Interface
Crack interaction
Spring stiffness
Ultrasound

ABSTRACT

An effective spring stiffness approximation is proposed for a hexagonal array of coplanar penny shaped cracks located at the interface between two dissimilar solids. The approximation is based on the factorization of the solution on the material dissimilarity factor, the crack interaction factor and the effective spring stiffness solution for non-interacting cracks in a homogeneous material. Such factorization is exact and was validated for 2D collinear cracks between two dissimilar solids. The crack interaction factor is obtained using a recently developed model for stress intensity factors for an array of coplanar penny shaped cracks in a homogeneous material; also the material dissimilarity function recently obtained for non-interacting penny shaped crack at the interface between two dissimilar materials is employed. The obtained solution is useful for an assessment by ultrasonic measurements of the interface stiffness in bonded structures for monitoring the interfacial microdamage growth due to mechanical loading and environmental factors.

1. Introduction

Bonded structures are widely used in various products and devices to improve structural durability and strength. The wide application of adhesive bonds in the aerospace industry for both aluminum and composite structures is well documented. In the field of dentistry, resin-retained ceramic restorations are performed to protect the remaining teeth and restore mechanical function without loss of aesthetics (Wang et al., 2007). Bonded interfaces are often compromised due to imperfect bonding conditions and degradation over time caused by various mechanical/thermal loadings and environmental factors. Micromechanical interfacial damage such as micro-cracks or micro-disbonds forms at the interfacial region and threatens the overall structural integrity.

Ultrasound methods are widely used to detect nondestructively different types of interfacial damage (Buck et al., 1989; Thompson and Thompson, 1991; Wang and Rokhlin, 1991; Margetan et al., 1992; Nagy, 1992; Rokhlin et al., 2004; Katoh et al., 2002; Milne et al., 2011). One approach in modeling elastic wave interaction with planar defects at the interface, such as micro-cracks or micro-disbonds, is to replace the microdefects-induced reduction in static stiffness by a continuous, uniform distribution of springs at the interface (Baik and Thompson, 1984; Sotiropoulos and Achenbach, 1988; Margetan et al., 1988; Lavrentyev and Rokhlin, 1994; Drinkwater et al., 1996; Delsanto and Scalerandi, 1998; Baltazar et al., 2003). This quasi-static approximation is demonstrated to be effective in modeling wave interactions at low frequencies, where the size of the damage is much smaller than the wavelength (Angel and Achenbach, 1985). The second approach is applicable when an interphase of finite thickness is formed because of material processing. This interphase has is its own constitutive properties affected by microdefects and if the microdefects are smaller than the interphase thickness their effect can be described by effective elastic properties (see for example Kachanov, 1994). Next, often when the wavelength is larger than the original layer thickness, an interphase between two media is replaced by an infinitely thin interface with appropriate boundary conditions, which is advantageous in solving the wave interaction problem (Rokhlin and Wang, 1991; Rokhlin and Huang, 1993; Hudson et al., 1997; Singher et al., 1994; Benveniste, 2006). For comparison of those two approaches see, for example, Lavrentyev and Rokhlin (1994) and Liu et al. (2000).

The objective of this work is to analyze the planar microdefects (microdisbonds) on an interface between two different solids. Such

* Corresponding author. Tel.: +1 614 292 0971; fax: +1 614 292 3163.
E-mail address: katsube.1@osu.edu (N. Katsube).
[1] Current address: Department of Mechanical Engineering, Bursa Technical University, Ataturk Kongre Kultur Merkezi, Merinos Parki, Osmangazi Bursa, Turkey.

0020-7683/$ - see front matter © 2013 Elsevier Ltd. All rights reserved.
http://dx.doi.org/10.1016/j.ijsolstr.2013.04.006

defects are modeled as an array of planar cracks, which are replaced by a continuum distribution of artificial springs at the interface, where the springs are selected in such a way that the stiffness reduction of the interface under far field loading is equivalent to that of the interface with an array of cracks. In order to be able to assess the bond integrity and the remaining life, accurate estimation of the percentage of disbond area (Palmer et al., 1988; Lavrentyev and Beals, 2000) is important. For this purpose, explicit expressions relating the spring stiffness constants to the crack geometry and density at the interface are desirable. For example, Baik and Thompson (1984) obtained the expression for effective normal spring stiffness for a planar array of periodically spaced strip cracks in a homogeneous material. They also obtained the corresponding expression for a single penny-shaped crack in a homogeneous material. Margetan et al. (1988) suggested an approximate expression for transverse spring stiffness for a single penny-shaped crack in a homogeneous material. Modifications of the Baik and Thompson (1984) and Margetan et al. (1988) methods were used by Lavrentyev and Rokhlin (1994) for an approximate description of an array of penny-shaped cracks between dissimilar materials in adhesive joints.

Most recently, Lekesiz et al. (2011a) obtained explicit analytical expressions for the normal and transverse effective spring stiffnesses of a planar periodic array of collinear cracks at an interface between two dissimilar isotropic materials based on the open crack model (Rice, 1988; Hutchinson and Suo, 1992). They (Lekesiz et al., 2011b) also obtained the normal and transverse spring stiffness expressions for a single penny-shaped crack at an interface between two dissimilar isotropic materials.

Most bonded interfaces consist of two dissimilar materials and micro-cracks or micro-disbonds at the interface are better represented by penny-shaped cracks than planar cracks. In addition, crack interactions play an important role in assessing the remaining life of bonded structures. Currently, however, there is no fracture mechanics based relationship between interfacial effective spring stiffness and crack density for interacting penny-shaped cracks at an interface between two dissimilar isotropic solids; such an approximate explicit relationship is obtained in this work.

2. Problem formulation for effective spring stiffness of cracked interface

The outline of our approach is presented schematically in Fig. 1. First, Fig. 1(a), the distributed effective interface spring stiffness is obtained to describe a periodic array of coplanar penny-shaped cracks between two identical elastic semispaces, and the effect of crack interactions on the spring stiffness is examined. For this, the array of planar cracks in the material is replaced by an artificial interface with a continuum distribution of springs utilizing our recent results (Lekesiz et al., 2013) where the effect of crack interactions on the stress intensity factors for a periodic array of coplanar penny-shaped cracks in a homogeneous material is obtained based on the approximate method by Kachanov and his co-workers (1985, 1987, 1989, 1994). Second, Fig. 1(b), the effect of material dissimilarity on the equivalent spring stiffness for a single (non-interacting) penny-shaped crack at an interface between two dissimilar materials is examined based on the work by Lekesiz et al. (2011b). Finally, similarly to the exact results by Lekesiz et al. (2011a) for an infinite array of 2D collinear cracks between two dissimilar solids, the effective spring stiffness is expressed in terms of three factors: crack interactions, material dissimilarity, and the spring stiffness of a single crack. Combining the crack interaction and material dissimilarity factors as shown in Fig. 1(a) and (b), respectively, and utilizing the effective spring stiffness for single penny shaped crack in a homogeneous material, we propose an approximate but explicit analytical expressions for equivalent spring stiffness for a periodic array of interacting penny-shaped cracks at an interface between two dissimilar materials as shown in Fig. 1(c).

The notion of the effective spring stiffness as depicted in Fig. 1 can be briefly described as follows. The far field displacement, Δ, can be separated into a displacement component without cracks, $\Delta_{no\text{-}crack}$, and an additional displacement due to the presence of cracks, Δ_{crack}, as follows.

$$\Delta = \Delta_{no-crack} + \Delta_{crack} \tag{1}$$

The idea (Baik and Thompson, 1984; Margetan et al., 1988; Lekesiz et al., 2011a) is to replace cracks by continuously distributed interfacial springs with the effective spring stiffness, k, such that they provide the same additional interface compliance (additional displacement Δ_{crack}) as that due to the cracks.

$$k_N = \frac{p^0}{\Delta_{N,crack}}, \quad k_T = \frac{t^0}{\Delta_{T,crack}} \tag{2}$$

where the subscripts N and T, respectively, denote the normal and transverse directions and p^0 and t^0, respectively, are the normal and shear traction applied at infinity.

The additional displacements can be determined using Castigliano's theorem, extended for cracked bodies (Tada et al., 2000), as in

$$\Delta_{N,crack} = \frac{\partial U_N}{\partial Q_N} \quad \Delta_{T,crack} = \frac{\partial U_T}{\partial Q_T} \tag{3}$$

where $Q_N = \pi b^2(p^0)$ and $Q_T = \pi b^2(t^0)$, respectively, represent the applied normal and transverse forces by considering the unit cylindrical cell with a circular cross sectional area $\pi\, b^2$ corresponding to the crack #1 region. The strain energies due to normal and shear tractions are respectively denoted by U_N and U_T. In obtaining the effective elastic spring stiffness for interacting coplanar penny-shaped cracks in a homogenous material in Eq. (2) (see Fig. 1(a)), we will first obtain the strain energy based on stress intensity factors, and then generalize this problem to the cracked interface between two solids.

3. Effective spring stiffness for a periodic array of interacting coplanar penny-shaped cracks at the interface between identical isotropic semispaces

3.1. Stress intensity factors

Consider a periodic array of coplanar penny-shaped cracks in an infinite medium subjected to remote normal and shear tractions as shown in Fig. 1(a). The hexagonal crack configurations (with crack radius a and crack periodicity b) as shown in Fig. 2(a) is considered. Lekesiz et al. (2013) numerically obtained the mode I, II and III stress intensity factors (SIFs), K_I, K_{II} and K_{III} for these interacting cracks as a function of crack density and the angle along the crack edge based on the approximate method developed by Kachanov and Laures (1989). The basic procedure for this analysis is summarized below.

The problem of N cracks subjected to remote tractions at infinity are replaced by equivalent problems where crack faces are loaded with normal and shear tractions, p^0 and t^0, respectively, and stresses vanishing at infinity. These equivalent problems with N cracks can be separated into N boundary value problems with each containing a single crack loaded by tractions which include crack interactions. Letting N go to infinity and using the fact that these N problems become identical, it is shown that the average traction for any crack (say crack #1) is magnified by a constant factor $\left(1 - \sum_{j=2}^{\infty} \Lambda_{j1}^{zz}\right)^{-1}$ due to crack interactions. The factor Λ_{j1}^{zz} is

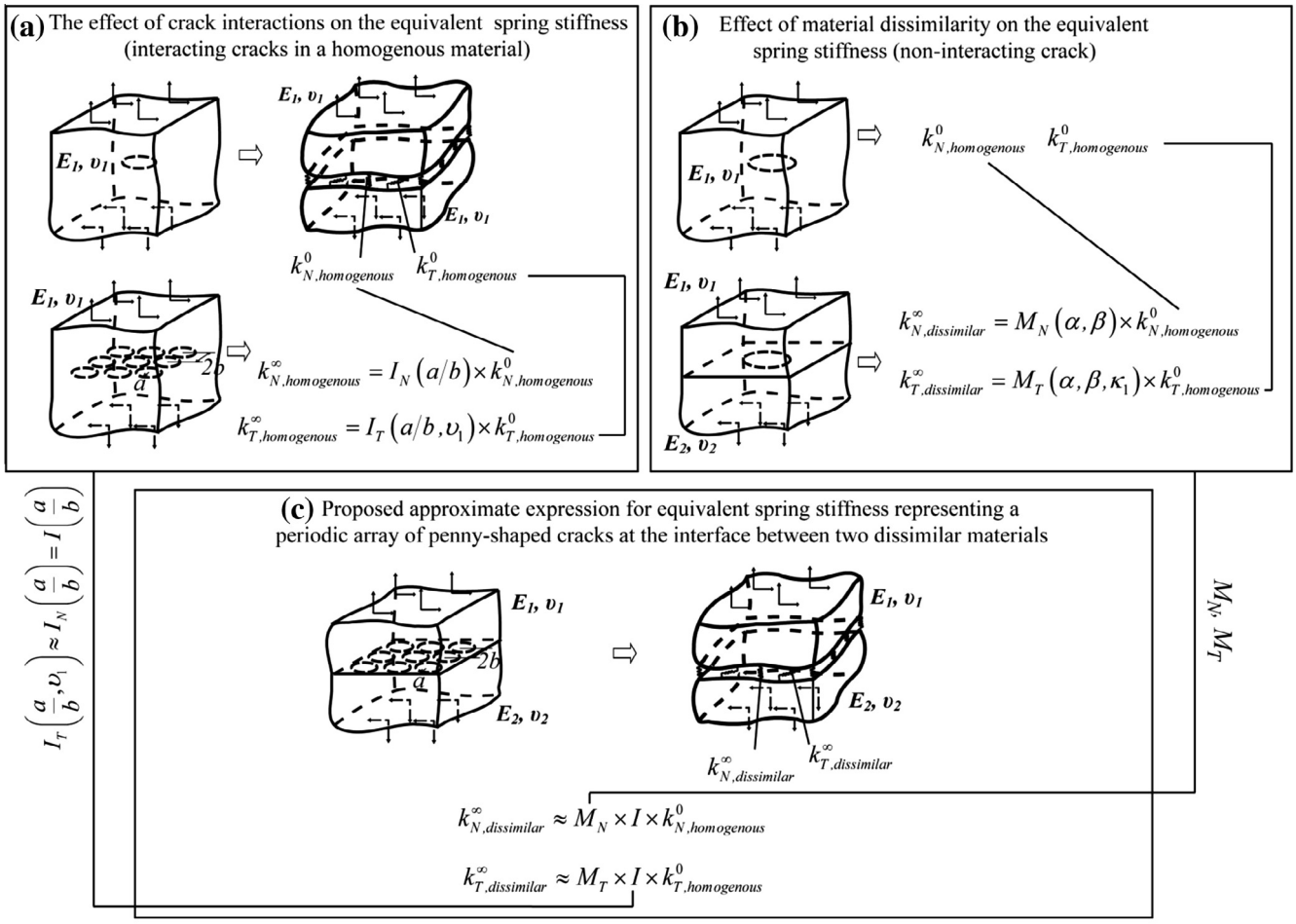

Fig. 1. Schematics of the work.

called the transmission factor (Kachanov, 1985, 1994) and describes the traction (in the z direction) averaged over the imaginary crack #1 region when a single crack #j in an infinite material is subjected to a unit uniform traction (in the z direction) at its crack faces as follows.

$$\Lambda^{zz}_{j1} = \frac{1}{\pi a^2}\int\int_{S_1}\overline{\sigma_j}(\overline{\rho_1},\phi_1)dS_1, \quad (j=1,2,3,\ldots) \tag{4}$$

where

$$\overline{\sigma_j}(\overline{\rho_j}) = \frac{2}{\pi}\left[\frac{1}{\sqrt{\left(\overline{\rho_j}^2-1\right)}} - \sin^{-1}\left(\frac{1}{\overline{\rho_j}}\right)\right] \tag{5}$$

In Eq. (4), the imaginary crack #1 region is represented by S_1, and the normalized radial distance and angle coordinate system, $\overline{\rho_1}(=\rho_1/a)$ and ϕ_1, are used as shown in Fig. 2(b). Eq. (5) represents the axisymmetric in-plane normal stress distribution outside the single crack #j as in Appendix A1 of Kachanov and Laures (1989) and Fabrikant (1990), and the corresponding normalized radial distance is denoted by $\overline{\rho_j}=\rho_j/a$. Following the work by Kachanov (1985) and Lekesiz et al. (2013) has shown that the traction of crack #1, which is the summation of the applied traction p^0 and the superposition of the effect of all surrounding cracks on crack #1, can be expressed as $p^0\left(1-\sum_{j=2}^{\infty}\Lambda^{zz}_{j1}\right)^{-1}\sum_{j=2}^{\infty}\overline{\sigma_j}$, resulting in the normalized mode I SIF as a function of ϕ as follows.

$$\frac{K^\infty_I(\phi)}{K^0_I} = \frac{1}{2\pi}\int_0^{2\pi}\int_0^1 \frac{\sqrt{1-\overline{\rho_1}^2}\left[1+\left(1-\sum_{j=2}^{\infty}\Lambda^{zz}_{j1}\right)^{-1}\sum_{j=2}^{\infty}\overline{\sigma_j}(\overline{\rho_1},\phi_1)\right]\overline{\rho_1}d\overline{\rho_1}d\phi_1}{1+\overline{\rho_1}^2-2\overline{\rho_1}\cos(\phi-\phi_1)} \tag{6}$$

where K^0_I is the SIF for single (non-interacting) crack loaded by a uniform normal traction, p^0, ($K^0_I = p^0\sqrt{2a}/\pi$), and the superscript, ∞, represents an infinite number of cracks.

A constant shear traction applied to an isolated single crack in the x direction produces a shear stress distribution in the x and y directions around that crack which affects the stress distribution in the vicinity of all other cracks. Due to this coupling, we need to consider the stress field around a single crack (crack #j) subjected to a constant shear, t^0 in the x direction and s^0 in the y direction. The shear stress distribution outside the crack is given by Eq. (44) in Sankar and Fabrikant (1983) as follows.

$$\tau^x_j(\overline{\rho_j},\phi_j) + i\tau^y_j(\overline{\rho_j},\phi_j) = \frac{2(t^0+is^0)}{\pi}\left[\frac{1}{\sqrt{\overline{\rho_j}^2-1}} - \sin^{-1}\frac{1}{\overline{\rho_j}}\right] + \frac{2(t^0-is^0)}{\pi} \times \frac{\upsilon}{2-\upsilon}\left(\frac{\cos 2\phi_j + i\sin 2\phi_j}{\overline{\rho_j}^2\sqrt{\overline{\rho_j}^2-1}}\right) \tag{7}$$

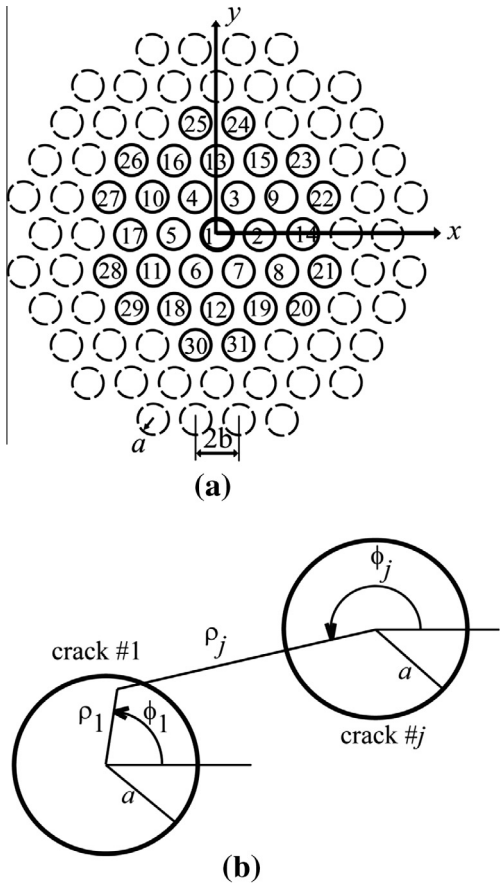

Fig. 2. (a) Hexagonal configuration of cracks, (b) Crack #1 coordinates and relation with crack #j coordinates.

where τ_j^x and τ_j^y, respectively, are the shear stresses in the x and y directions around the crack #j and υ represents the Poisson's ratio.

While the remote shear traction component s^0 is zero in our case, the traction distribution over the crack #1 surface area is shown to have both x and y components, t_1 and s_1, respectively as follows.

$$t_1(\overline{\rho}_{1,},\phi_1)=\left[t^0+\left(1-\sum_{j=2}^{\infty}\Lambda_{j1}^{zz}\right)^{-1}\sum_{j=2}^{\infty}\tau_j^x(\overline{\rho}_1,\phi_1)\Big|_{s^0=0}\right],$$
$$s_1(\overline{\rho}_{1,},\phi_1)=\left(1-\sum_{j=2}^{\infty}\Lambda_{j1}^{zz}\right)^{-1}\sum_{j=2}^{\infty}\tau_j^y(\overline{\rho}_{1,}\phi_1)|_{s^0=0} \tag{8}$$

In deriving Eq. (8), a key result related to the unique periodicity of crack configurations is used: the average shear stress in the x direction is magnified by the same constant factor $\left(1-\sum_{j=2}^{\infty}\Lambda_{j1}^{zz}\right)^{-1}$ as the normal traction, Eq. (6). This leads to expressions for the mode II and mode III SIFs for equivalent problems where crack faces are subjected to a shear, t^0, in the x direction as follows:

$$K_{II}^{\infty}(\phi)+iK_{III}^{\infty}(\phi)=\frac{\sqrt{a}}{\pi^2\sqrt{2}}\int_0^{2\pi}\int_0^1\sqrt{1-\overline{\rho}_1^2}\left\{\frac{e^{-i\phi}(t_1+is_1)}{1+\overline{\rho}_1^2-2\overline{\rho}_1\cos(\phi-\phi_1)}\right.$$
$$\left.+\frac{\upsilon}{2-\upsilon}\frac{e^{i\phi}(3-\overline{\rho}_1e^{i(\phi-\phi_1)})(t_1-is_1)}{(1-\overline{\rho}_1e^{i(\phi-\phi_1)})^2}\right\}\overline{\rho}_1d\overline{\rho}_1d\phi_1 \tag{9}$$

The effect of crack #j on crack #1 diminishes as the distance between two cracks becomes large in the infinite series in Eqs. (6), (8), and (9). Based on this, in Lekesiz et al. (2013), it is shown that for crack number larger than 31 in the hexagonal crack configuration (Fig. 2(a)), the effect of crack #j traction on the crack #1 region can be represented by the values at the center of crack #1, $\overline{\sigma_j}(\rho_1=0)$, $\overline{\tau_j^x}(\rho_1=0)$, $\overline{\tau_j^y}(\rho_1=0)$. An infinite number of cracks can be truncated at 10^9 cracks with possible convergence error less than 0.09% for the crack density range considered, $0<a/b<0.99$, and all values of Poisson's ratio.

3.2. Strain energy for interacting cracks

The total crack strain energy for a three-dimensional crack (Sih, 1973) can be expressed as

$$U=2\pi\int_A\left\{\frac{(1-\upsilon^2)}{E}\left(K_I^2+K_{II}^2\right)+\frac{(1+\upsilon)}{E}K_{III}^2\right\}dA \tag{10}$$

where A represents the crack area. The above equation is obtained based on the Griffith–Irwin energy balance theory of crack extension where the energy made available per unit increase in crack surface area (energy release rate) results from the work from displacements of loading forces and/or reductions in strain energy in a body accompanying a unit increase in crack area. Note that the SIFs in Eq. (10) are based on the definition used by Kachanov and Laures (1989) and differ from those used by Sih (1973) by a factor of $\sqrt{2\pi}$.

Taking the mode I; II and III SIFs for a single crack (Sih, 1973) denoted by K_I^0, $K_{II}^0(\phi)$ and $K_{III}^0(\phi)$ as:

$$K_I^0=\frac{p^0\sqrt{2a}}{\pi};\quad K_{II}^0(\phi)=\frac{2t^0\sqrt{2a}}{\pi(2-\upsilon)}\cos\phi;$$
$$K_{III}^0(\phi)=\frac{2t^0(1-\upsilon)\sqrt{2a}}{\pi(2-\upsilon)}\sin\phi \tag{11}$$

and using them to evaluate strain energy for the normal U_N^0 and transverse U_T^0 loading modes of a single penny-shape crack we obtain

$$U_N^0=\frac{(1-\upsilon^2)}{E}\frac{4(p^0)^2}{\pi}b^3\left[\frac{2\pi}{3}\left(\frac{a}{b}\right)^3\right] \tag{12}$$

$$U_T^0=\frac{16(t^0)^2(1-\upsilon^2)}{\pi(2-\upsilon)^2E}b^3\left[\frac{(2-\upsilon)\pi}{3}\left(\frac{a}{b}\right)^3\right] \tag{13}$$

Now considering an infinite array and separating the total crack strain energy U into terms for the mode I, U_N^{∞}, and the mode II and III, U_T^{∞}, contributions (the superscript, ∞, are added to emphasize an infinite number of coplanar cracks) and normalizing them by the corresponding quantities for a single non-interacting crack U_N^0, U_T^0 we obtain

$$\frac{U_N^{\infty}}{U_N^0}=\frac{\int_0^{2\pi}\int_0^{a/b}\left[\frac{K_I^{\infty}(\phi,\bar{r})}{K_I^0(\phi,\bar{r})}\right]^2\bar{r}^2d\bar{r}d\phi}{\frac{2\pi}{3}\left(\frac{a}{b}\right)^3} \tag{14}$$

and

$$\frac{U_T^{\infty}}{U_T^0}=\frac{\int_0^{2\pi}\int_0^{a/b}\left\{\left[\frac{K_{II}^{\infty}(\phi,\bar{r})}{K_{II}^0(\phi,\bar{r})}\right]^2(\cos\phi)^2+(1-\upsilon)\left[\frac{K_{III}^{\infty}(\phi,\bar{r})}{K_{III}^0(\phi,\bar{r})}\right]^2(\sin\phi)^2\right\}\bar{r}^2d\bar{r}d\phi}{\frac{(2-\upsilon)\pi}{3}\left(\frac{a}{b}\right)^3} \tag{15}$$

where $\bar{r}=r/b$ is employed to integrate the energy release rate over the entire crack area.

Those normalized normal and transverse crack strain energies for an array of cracks, Eqs. (14) and (15) represent crack interactions. The forms of these two equations are significantly different in the sense that Eq. (15) (the normalized transverse crack strain

energy) depends on Poisson's ratio υ while Eq. (14) (the normalized normal crack strain energy) is independent of Poisson's ratio. The Poisson's ratio dependence of numerical values of Eq. (15), however, vanishes.

In order to elucidate this point, two terms in the integrand of Eq. (15) $\left[\frac{K_{II}^{\infty}(\phi,\bar{r})}{K_{II}^{0}(\phi,\bar{r})}\right]^2(cos\phi)^2\bar{r}^2$, $\left[\frac{K_{III}^{\infty}(\phi,\bar{r})}{K_{III}^{0}(\phi,\bar{r})}\right]^2(\sin\phi)^2\bar{r}^2$ are plotted in Fig. 3(a) and (b) as a function of ϕ for the cases $\bar{r}=0.75$, 0.95, 0.99 with Poisson's ratio $\upsilon=0$, 0.3, 0.5. It is clear that these terms are dependent on Poisson's ratio. However, after integration of these terms with respect to $\bar{r}$ and ϕ the resulting integral terms become identical to one half of the numerator of Eq. (14), $\frac{1}{2}\int_0^{2\pi}\int_0^{a/b}\left[\frac{K_I^{\infty}(\phi,\bar{r})}{K_I^{0}(\phi,\bar{r})}\right]^2\bar{r}^2d\bar{r}d\phi$, which is independent of Poisson's ratio. All three integral terms are plotted in Fig. 3(c); they are indistinguishable within the precision of Fig 3 for all values of υ despite the fact that the integrands do depend on Poisson's ratio as shown in Fig. 3(a) and (b). Some selected values of these three integral terms are listed in Table 1, and for all values of υ the maximum difference among them remains less than 0.7%, which occurs when $\upsilon=0.5$ and $a/b=0.99$. Considering the approximation involved in evaluation of the SIFs related to Kachanov's method itself and numerical errors related to truncation of number of cracks, we attributed the maximum 0.7% error to approximations of the numerical method employed in our work. The analytical proof of the exact independence of these integrals on υ was not obtained in this work, and we accept an approximate equality which is suitable for all practical purposes as follows from Fig. 3(c):

$$\begin{aligned}&\int_0^{2\pi}\int_0^{a/b}\left[\frac{K_{II}^{\infty}(\phi,\bar{r})}{K_{II}^{0}(\phi,\bar{r})}\right]^2(\cos\phi)^2\bar{r}^2d\bar{r}d\phi\\&\approx\int_0^{2\pi}\int_0^{a/b}\left[\frac{K_{III}^{\infty}(\phi,\bar{r})}{K_{III}^{0}(\phi,\bar{r})}\right]^2(\sin\phi)^2\bar{r}^2d\bar{r}d\phi\\&\approx\frac{1}{2}\int_0^{2\pi}\int_0^{a/b}\left[\frac{K_{I}^{\infty}(\phi,\bar{r})}{K_{I}^{0}(\phi,\bar{r})}\right]^2\bar{r}^2d\bar{r}d\phi\end{aligned}\tag{16}$$

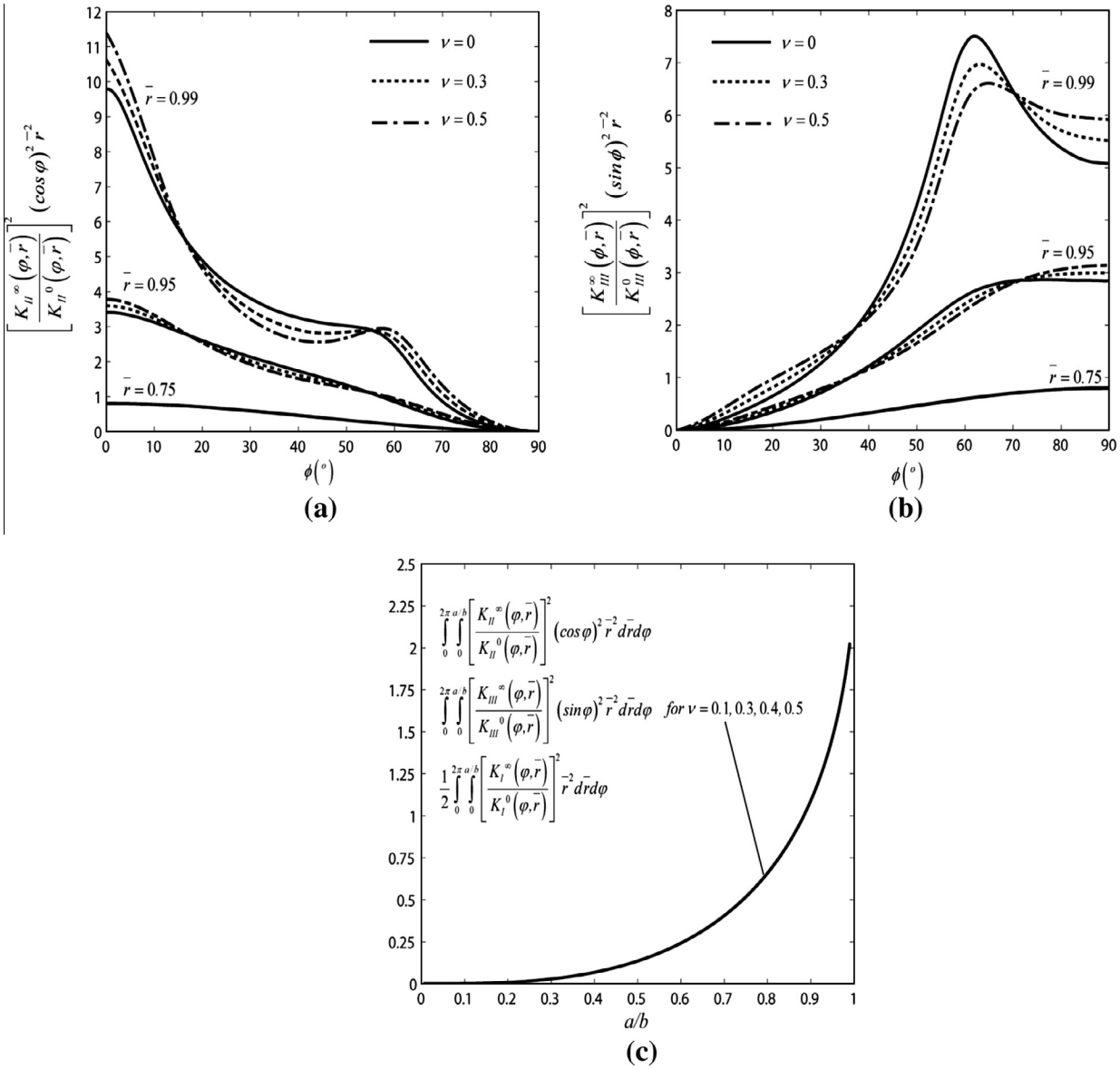

Fig. 3. (a) $\left[\frac{K_{II}^{\infty}(\phi,\bar{r})}{K_{II}^{0}(\phi,\bar{r})}\right]^2(\cos\phi)^2\bar{r}^2$, (b) $\left[\frac{K_{III}^{\infty}(\phi,\bar{r})}{K_{III}^{0}(\phi,\bar{r})}\right]^2(\sin\phi)^2\bar{r}^2$, as a function of φ for the case of $\bar{r}=0.75$, 0.95, 0.99 with parameter $\nu=0$, 0.3, 0.5. (c) $\int_0^{2\pi}\int_0^{a/b}\left[\frac{K_{II}^{\infty}(\phi,\bar{r})}{K_{II}^{0}(\phi,\bar{r})}\right]^2(\cos\phi)^2\bar{r}^2d\bar{r}d\phi$, $\int_0^{2\pi}\int_0^{a/b}\left[\frac{K_{III}^{\infty}(\phi,\bar{r})}{K_{III}^{0}(\phi,\bar{r})}\right]^2(\sin\phi)^2\bar{r}^2d\bar{r}d\phi$, and $\frac{1}{2}\int_0^{2\pi}\int_0^{a/b}\left[\frac{K_{I}^{\infty}(\phi,\bar{r})}{K_{I}^{0}(\phi,\bar{r})}\right]^2\bar{r}^2d\bar{r}d\phi$ as a function of a/b.

Table 1
Selected values of integrals in Eqs. (14) and (15) shown in Fig. 3(c) with parameters a/b and υ.

		$a/b = 0.3$	$a/b = 0.5$	$a/b = 0.7$	$a/b = 0.9$	$a/b = 0.99$
$\int_0^{2\pi}\int_0^{a/b}\left[\frac{K_{II}^{\infty}(\phi,\bar{r})}{K_{II}^{0}(\phi,\bar{r})}\right]^2(\cos\phi)^2\bar{r}^2d\bar{r}d\phi$	$\upsilon = 0.1$	0.028377	0.13566	0.40570	1.0915	2.0221
	$\upsilon = 0.3$	0.028388	0.13571	0.40585	1.0921	2.0253
	$\upsilon = 0.4$	0.028398	0.13574	0.40599	1.0925	2.0277
	$\upsilon = 0.5$	0.028402	0.13578	0.40607	1.0928	2.0305
$\int_0^{2\pi}\int_0^{a/b}\left[\frac{K_{III}^{\infty}(\phi,\bar{r})}{K_{III}^{0}(\phi,\bar{r})}\right]^2(\sin\phi)^2\bar{r}^2d\bar{r}d\phi$	$\upsilon = 0.1$	0.028362	0.13558	0.40548	1.0910	2.0202
	$\upsilon = 0.3$	0.028344	0.13550	0.40523	1.0903	2.0184
	$\upsilon = 0.4$	0.028329	0.13542	0.40501	1.0897	2.0172
	$\upsilon = 0.5$	0.028308	0.13533	0.40472	1.0890	2.0166
$\frac{1}{2}\int_0^{2\pi}\int_0^{a/b}\left[\frac{K_{I}^{\infty}(\phi,\bar{r})}{K_{I}^{0}(\phi,\bar{r})}\right]^2\bar{r}^2d\bar{r}d\phi$		0.028368	0.13561	0.40556	1.0911	2.0210

Due to the equality (16) in Eq. (15), numerical values of normalized strain energies U_N^{∞}/U_N^0; U_T^{∞}/U_T^0 (Eqs. (14) and (15)) become nearly identical and independent of Poisson's ratio. This numerical result may be attributed to the periodicity of the crack configuration where, as discussed in Section 3.1, the average shear stress in the x direction is magnified by the same constant factor as for the normal traction.

In Fig. 4(a) the normalized strain energies, Eqs. (14) and (15), are plotted as a function of a/b; both equation plots are indistinguishable for all values of a/b and independent of the Poisson's ratio υ. As the crack density, a/b, increases, the normalized crack strain energy increases indicating large crack interactions. The maximum values of the normalized strain energy reaches 2.16 as a/b approaches one.

3.3. Comparison with normalized crack strain energy for two interacting coplanar cracks

Problems of two interacting coplanar cracks have been extensively investigated. Fabrikant (1987, 1989) have obtained integral equations and numerically investigated normal and transverse crack energy ratios for two closely interacting coplanar cracks, U_N^{two}/U_N^0 and U_T^{two}/U_T^0 (superscript *two* indicates two cracks). Kachanov and Laures (1989) produced the mode I, II and III SIFs for two closely interacting coplanar cracks using the approximate method outlined in Section 3.1 and verified the results against the results produced by Fabrikant (1987, 1989).

In order to examine differences between crack interactions for an array of infinite number of coplanar cracks and those for two cracks, the normal and transverse crack strain energy for two interacting coplanar cracks normalized by the corresponding strain energy for non-interacting cracks have been computed using the Kachanov and Laures (1989) method. The results obtained are plotted in Fig. 4(b) (curves) together with the exact results (points) numerically obtained by Fabrikant (1987, 1989); Poisson's ratio is $\upsilon = 0.5$. As in the case for an array of infinite cracks, the normalized strain energy for two cracks increases with a/b; however, the maximum value of the normalized transverse crack strain energy is 1.115 (Fig. 4(b)) and about twice smaller than that for an infinite number of cracks, 2.16 (Fig. 4(a)). This indicates significantly stronger interaction of an infinite number of cracks.

An another important point is that for an array of infinitely many cracks the normalized transverse and normal crack strain energies are practically identical for all values of υ (Fig. 4(a)), where the normalized transverse crack strain energy for two cracks, at $\upsilon = 0.5$, is larger than the normalized normal crack strain energy. Only when $\upsilon = 0$ do the normalized transverse and normal crack strain energies for two cracks become identical. This difference can be attributed to the fact that two coplanar cracks lack the periodic nature and symmetry that characterize the behavior of an infinite array of cracks as discussed in Section 3.2.

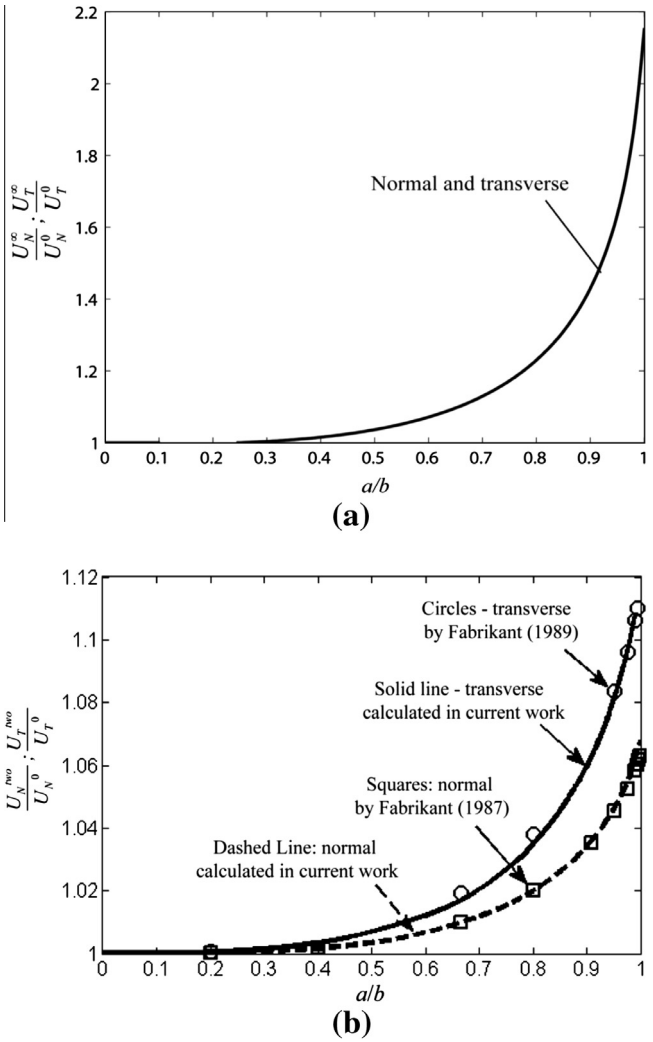

Fig. 4. Crack strain energy in the normal and transverse directions for multiple coplanar penny-shaped cracks normalized by those for non-interacting crack: (a) an array of infinite number of cracks for all values of υ; (b) two cracks for the case of $\upsilon = 0.5$, comparison of calculated values in this work and those given by Fabrikant (1987,1989).

3.4. Effective spring stiffness for an infinite hexagonal array of cracks

In this section, the effective spring stiffness expressions for a hexagonal array of coplanar penny-shaped cracks (Figs. 1 and 2(a)) are derived based on the crack energy expressions discussed in Section 3.2.

By inserting Eqs. (14), (15), (12), and (13) into Eqs. (2) and (3), the normal and transverse spring stiffness for an array of cracks, $k_{N,homogenous}^{\infty}$ and $k_{T,homogenous}^{\infty}$ (the subscript, homogeneous, and the

superscript, ∞, are added to emphasize an infinite number of coplanar cracks in a homogeneous material) are obtained as follows.

$$k^{\infty}_{N,homogenous} = \frac{\pi^2}{8b}\frac{E}{(1-\upsilon^2)}\left[\int_0^{2\pi}\int_0^{a/b}\left(\frac{K^{\infty}_I}{K^0_I}\right)^2 \bar{r}^2 d\bar{r}d\phi\right]^{-1} \tag{17}$$

$$k^{\infty}_{T,homogenous} = \frac{\pi^2}{32b}\frac{E(2-\upsilon)^2}{(1-\upsilon^2)} \left[\int_0^{2\pi}\int_0^{a/b}\left\{\left(\frac{K^{\infty}_{II}}{K^0_{II}}\right)^2(\cos\phi)^2 + (1-\upsilon)\left(\frac{K^{\infty}_{III}}{K^0_{III}}\right)^2(\sin\phi)^2\right\}\bar{r}^2 d\bar{r}d\phi\right]^{-1} \tag{18}$$

As a/b approaches zero, the equivalent spring stiffness for a periodic array of infinite cracks approaches that for a non-interacting single crack. By setting the SIF ratios in Eqs. (17) and (18) equal to one $\left(K^{\infty}_I/K^0_I = K^{\infty}_{II}/K^0_{II} = K^{\infty}_{III}/K^0_{III} = 1\right)$, the equivalent normal and transverse spring stiffness for a single crack are recovered as a special case:

$$k^0_{N,homogenous} = \frac{3\pi}{16b}\frac{E}{(1-\upsilon^2)}\left(\frac{a}{b}\right)^{-3} \tag{19}$$

$$k^0_{T,homogenous} = \frac{3\pi}{32b}\frac{E}{(1-\upsilon^2)}(2-\upsilon)\left(\frac{a}{b}\right)^{-3} \tag{20}$$

where the subscript, 0, indicates an isolated single crack. These are identical to the spring stiffness for an isolated crack obtained by Margetan et al. (1988).

3.5. Crack interaction function for an infinite array of penny-shaped cracks

As for the normalized crack strain energy in Eqs. (14) and (15), the normal and transverse spring stiffness expressions for an array of an infinite number of cracks normalized by those for a single crack represent crack interactions. We introduce the normal and tangential crack interaction functions, I^{∞}_N and I^{∞}_T, respectively defined by the normalized normal and transverse stiffness expressions, and they are shown to be the inverse of crack energy ratios as follows.

$$I^{\infty}_N\left(\frac{a}{b}\right) = \frac{k^{\infty}_{N,homogenous}}{k^0_{N,homogenous}} = \left(\frac{U^{\infty}_N}{U^0_N}\right)^{-1} \tag{21}$$

and

$$I^{\infty}_T\left(\frac{a}{b}\right) = \frac{k^{\infty}_{T,homogenous}}{k^0_{T,homogenous}} = \left(\frac{U^{\infty}_T}{U^0_T}\right)^{-1} \tag{22}$$

Since the normalized normal and transverse crack strain energy, U^{∞}_N/U^0_N and U^{∞}_T/U^0_T, are identical for all practical purposes as discussed in Section 3.2, we can drop the subscripts N and T as follows.

$$I^{\infty}_N\left(\frac{a}{b}\right) = \frac{\frac{2\pi}{3}\left(\frac{a}{b}\right)^3}{\int_0^{2\pi}\int_0^{a/b}\left[\frac{K^{\infty}_I(\phi,\bar{r})}{K^0_I(\phi,\bar{r})}\right]^2\bar{r}^2 d\bar{r}d\phi} \approx I^{\infty}_T\left(\frac{a}{b}\right) \approx I^{\infty}\left(\frac{a}{b}\right) \tag{23}$$

Recently Lekesiz et al. (2011a) have obtained explicit analytical expressions for the normal and transverse effective spring stiffnesses of a planar infinite periodic array of collinear two-dimensional cracks at the interface between two dissimilar isotropic materials; both normal and transverse spring stiffness are shown to be identical. They have also shown that the crack interaction depends weakly on material dissimilarity, and for this reason for most practical cases the crack interaction is nearly the same as that for an array of collinear two-dimensional strip cracks between identical solids and can be expressed as follows (Eq. (33) in Lekesiz et al. (2011a)).

$$I^{2-D}\left(\frac{a}{b}\right) = \frac{\pi^2}{8}\left(\frac{a}{b}\right)^2\left[\ln\left\{\sec\left(\frac{\pi a}{2b}\right)\right\}\right]^{-1} \tag{24}$$

where $2a$ is the full crack length and $2b$ is the periodicity (the distance between the center of two adjacent cracks) and the superscript, 2-D, is added to emphasize 2D strip cracks. Eqs. (23) and (24) are a measure of the reduction in the effective spring stiffness due to crack interactions and may vary from one (no crack interaction) to zero (zero spring stiffness).

Motivated by the form of the interaction function for a periodic array of strip cracks given by Eq. (24), the numerically evaluated interaction function for the hexagonal configuration (Eq. (23) was curve fitted by the least square method. This leads to the following approximate analytical expression.

$$I^{\infty}\left(\frac{a}{b}\right) \approx C\frac{\pi^2}{8}\left(\frac{a}{b}\right)^{3.5}\left(\ln\left\{\sec\left[\frac{\pi}{2}\sqrt{C}\left(\frac{a}{b}\right)^{1.75}\right]\right\}\right)^{-1} \tag{25}$$

where $C = 0.8673$. The maximum curve fitting error is less than 0.5% for all values of a/b. The interaction function $I^{\infty}_N(a/b)$ Eq. (23) and the curve-fitted approximate function Eq. (25) are plotted in Fig. 5(a); they are indistinguishable within the accuracy of the figure.

By recalling Eqs. (19), (20), and (23) and inserting Eq. (25) into Eqs. (21) and (22), the normal $k^{\infty}_{N,homogeneous}$ and transverse $k^{\infty}_{T,homogeneous}$ spring stiffnesses for the periodic array of coplanar penny-shaped cracks in a homogenous material are obtained as follows:

$$k^{\infty}_{N,homogenous} \approx \frac{3\pi^3 C}{128b}\frac{E}{(1-\upsilon^2)} \times\sqrt{\left(\frac{a}{b}\right)}\left(\ln\left\{\sec\left[\frac{\pi}{2}\sqrt{C}\left(\frac{a}{b}\right)^{1.75}\right]\right\}\right)^{-1} \tag{26}$$

and

$$k^{\infty}_{T,homogenous} \approx \frac{3\pi^3 C}{256b}\frac{E(2-\upsilon)}{(1-\upsilon^2)} \times\sqrt{\left(\frac{a}{b}\right)}\left(\ln\left\{\sec\left[\frac{\pi}{2}\sqrt{C}\left(\frac{a}{b}\right)^{1.75}\right]\right\}\right)^{-1} \tag{27}$$

3.6. Comparison of crack interaction function $I^{\infty}(a/b)$ with other models

Based on a cylindrical unit cell model with a center crack by Tada et al. (2000) and Margetan et al. (1988) have obtained approximate normal and transverse effective spring stiffnesses for the special case of weakly interacting cracks (low crack density) in the square crack configuration. Normalizing their approximate results (Eqs. (3)(a) and (b) in Margetan et al., 1988) by the spring stiffness for a single crack, the corresponding interaction function for the normal and transverse effective spring stiffness can be shown to be identical and expressed as:

$$I^{\infty}_{Margetan}(A_d) = \frac{1}{3}A_d^{3/2}\Big[1.299723A_d^{1/2} - 0.9952365A_d + 0.66720233A_d^{3/2} - 0.42308925A_d^2 + 0.1406982A_d^{5/2} - 0.02954016A_d^3 + \frac{0.149058A_d^{1/2}}{1+A_d^{1/2}} - 1.868685\ln\left(1+A_d^{1/2}\right) - 0.419904\ln\left(1-A_d^{1/2}\right)\Big]^{-1} \tag{28}$$

where $A_d = (\pi a^2)/(4b^2)$ represents the areal crack density for the square configuration. The subscript, *Margetan*, is added to emphasize that this expression is based on Margetan et al. (1988) and the superscript, ∞, is added to emphasize the infinite number of coplanar penny-shaped cracks.

The interaction functions $I^{2-D}\left(\frac{a}{b}\right)$ (Eq. (24)), $I^{\infty}\left(\frac{a}{b}\right)$ (Eq. (25)) and $I^{\infty}_{M\ argetan}\left(\frac{a}{b}\right)$ (Eq. (28)) are plotted as a function of crack density parameter a/b in Fig. 5(a). As a/b approaches one, the interaction function for strip cracks, $I^{2\text{-D}}$, approaches zero since two semi-spaces in the plane of cracks will be completely separated. The minimum value of the interaction function for the hexagonal array of penny-shaped cracks, I^{∞}, however, is 0.43 since some connected regions remain. For all values of a/b, the crack interaction for strip cracks is significantly larger than for penny-shaped cracks (stronger deviation from non-interactive case, unity).

The relative difference between the interaction function based on the approximate unit cell model by Margetan et al. (1988), $I^{\infty}_{Margetan}$, and those based on this work for the hexagonal configurations, I^{∞}, is plotted in Fig. 5(b). The crack interaction for the unit cell model by Margetan et al. (1988) is smaller than that for the hexagonal configuration obtained in this work. The difference is small for small crack density but it increases with a/b, reaching a maximum, 15 as a/b approaches one. Some of this difference obviously may come from the difference in crack pattern (the square crack configuration in Margetan et al. (1988) vs. the hexagonal crack configuration considered in this work). It is important to note that the model of Margetan et al. (1988) is based on many simplified assumptions that are difficult to justify. The remarkable fact that their solution is close, at least for small crack density, to that of this work supports their assumptions which can be extended for other configuration of cracks.

Strip cracks and penny-shaped cracks may be considered as two extreme limiting cases of elliptical cracks. Crack interactions in terms of the SIFs for two coplanar elliptical cracks subjected to constant normal and shear tractions show similar behavior for different aspect ratio (Roy and Chatterijee, 1994; Saha et al., 1999), suggesting that the corresponding interaction function for spring stiffness may share a common form.

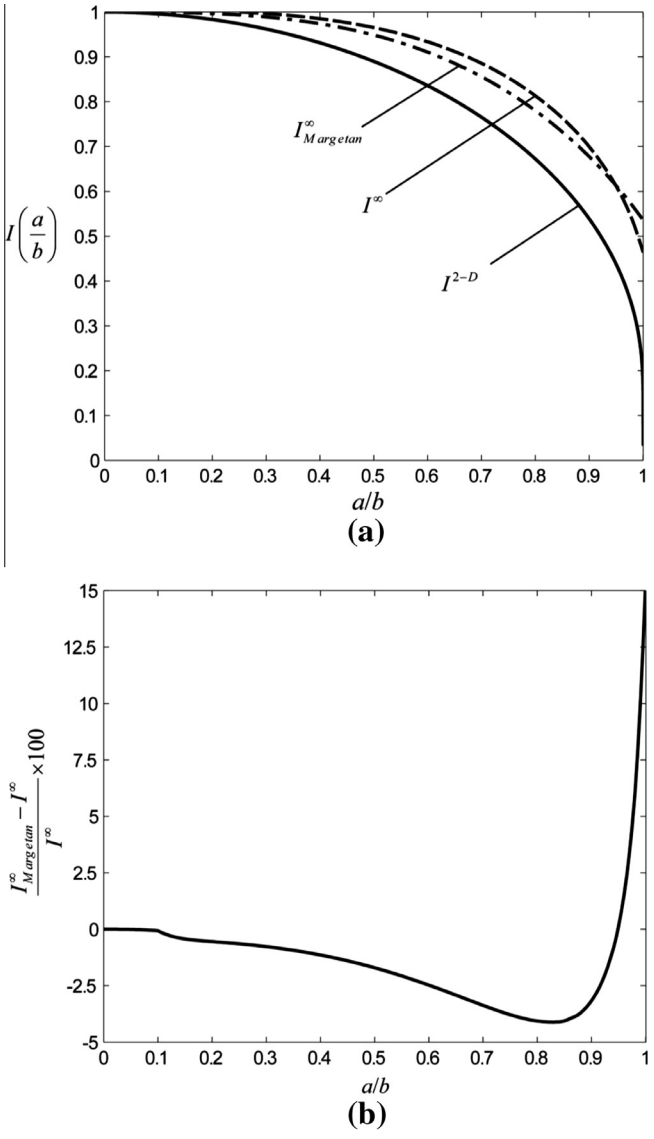

Fig. 5. (a) Comparison of Interaction functions: a hexagonal array of penny-shaped cracks obtained in this work, I^{∞} (Eq. (23) and (25)), a square array based on the approximate unit cell model (Margetan et al. (1988)), $I^{\infty}_{Magetam}$ (Eq.(28)), a periodic array of 2-D strip cracks, $I^{2\text{-D}}$ (Eq. (24)), (b) relative percent difference between $I^{\infty}_{Magetam}$ and I^{∞}.

4. Spring stiffness for a periodic array of penny-shaped cracks at the interface between two dissimilar isotropic materials

4.1. Proposed factorization of spring stiffness as material and interaction functions

In Lekesiz et al. (2011a), explicit analytical expressions for the normal and transverse effective spring stiffness for a planar periodic array of two-dimensional collinear cracks at an interface between two dissimilar isotropic materials was obtained. The crack interaction depends weakly on material dissimilarity and is nearly the same as that for crack arrays between two identical solids (see Eq. (24) in Section 3.5). It was further shown by Lekesiz et al. (2011a) that this permits approximate factorization of the effective stiffness for a 2D array of cracks between dissimilar materials in terms of a product of an elastic dissimilarity factor, depending on two dissimilar material properties, and two factors obtained for cracks in a homogeneous material: the effective spring stiffness for a single crack and the crack interaction function.

We propose to apply this notion of approximate factorization for the effective spring stiffness of a periodic array of penny-shaped cracks at the interface between two dissimilar isotropic materials shown in Fig. 1(c). First we rewrite Eqs. (21) and (22) based on equality (23) as

$$k^{\infty}_{N,homogeneous} \approx I^{\infty}\left(\frac{a}{b}\right) \times k^{0}_{N,homogeneous};$$
$$k^{\infty}_{T,homogeneous} \approx I^{\infty}\left(\frac{a}{b}\right) \times k^{0}_{T,homogeneous} \tag{29}$$

where the explicit expression (25) for the interaction function $I^{\infty}(a/b)$ is used.

As shown in Fig. 5(a), the crack interaction is weaker for the 3D array of penny-shaped cracks than for the 2D crack array. Combined this fact with the weak dependence of crack interactions on the material dissimilarity as demonstrated by Lekesiz et al. (2011a), we conjecture that the dependence of 3D crack interactions between two dissimilar materials depends weakly on the material dissimilarity, and therefore it can be approximated by the interaction function $I^{\infty}\left(\frac{a}{b}\right)$ for a homogeneous material. This leads to the approximate representation of the normal $k^{\infty}_{N,dissimilar}$ and transverse $k^{\infty}_{T,dissimilar}$ spring stiffness for a periodic array of penny shaped cracks between two dissimilar materials in terms of the corresponding spring stiffness for single crack between two dissimilar materials, denoted by $k^{0}_{N,dissimilar}$ and $k^{0}_{T,dissimilar}$ respectively, factored by the interaction function:

$$k^{\infty}_{N,dissimilar} \approx I^{\infty}\left(\frac{a}{b}\right) \times k^{0}_{N,dissimilar},$$
$$k^{\infty}_{T,dissimilar} \approx I^{\infty}\left(\frac{a}{b}\right) \times k^{0}_{T,dissimilar} \tag{30}$$

4.2. Elastic dissimilarity function

Based on the work by Willis (1972), Lekesiz et al. (2011b) have obtained the normal $k^{0}_{N,dissimilar}$ and transverse $k^{0}_{T,dissimilar}$ effective spring stiffness for a single penny-shaped crack at an interface between two dissimilar, isotropic, linearly elastic materials (Fig. 1(b)) as:

$$k^{0}_{N,dissimilar} = \frac{3\pi}{16b}\left(\frac{a}{b}\right)^{-3}\frac{E_1}{(1-\upsilon_1^2)}\frac{(1+\alpha)\beta}{\pi\varepsilon(1+\varepsilon^2)(1-\beta^2)} \tag{31}$$

$$k^{0}_{T,dissimilar} = \frac{3\pi}{128b}\left(\frac{a}{b}\right)^{-3}\frac{E_1}{(1-\upsilon_1^2)} \times \frac{(1+\alpha)}{\gamma}\left[1+\frac{4\beta\gamma}{\pi\varepsilon(1+\varepsilon^2)(1-\beta^2)}\right] \tag{32}$$

where

$$\alpha = \frac{G_2(\kappa_1+1)-G_1(\kappa_2+1)}{G_2(\kappa_1+1)+G_1(\kappa_2+1)},$$
$$\beta = \frac{G_2(\kappa_1-1)-G_1(\kappa_2-1)}{G_2(\kappa_1+1)+G_1(\kappa_2+1)}, \quad \varepsilon = \frac{1}{2\pi}\log\left\{\frac{1+\beta}{1-\beta}\right\},$$
$$\gamma = \frac{G_1+G_2}{G_2(\kappa_1+1)+G_1(\kappa_2+1)} \tag{33}$$

Here, α, β are the so-called Dundurs' parameters (Dundurs, 1967; Dundurs and Bogy, 1969) that are expressed in terms of $\kappa_i = 3-4\upsilon_i$ (υ_i is Poisson's ratio, $i = 1, 2$ for the semi-space materials 1 and 2) and shear modulus G_i ($i = 1,2$). The range of these non-dimensional parameters for all material combinations are $\alpha[-1,1]$, $\beta[-0.5,0.5]$, $\varepsilon[-0.1748,0.1748]$ and $\gamma[0.25,0.5]$. By letting α and β approach zero in Eqs. (31) and (32), the normal and transverse effective spring stiffnesses for a single crack in a homogeneous material, Eqs. (19) and (20), are recovered.

Equations (31) and (32) were obtained based on Willis' solution (1972), which is known to exhibit an oscillatory crack interpenetration zone at the crack tips for transverse loading, thus special care was taken to obtain the valid loading range to avoid this problem. It has been shown, however, that the transverse spring stiffness Eq. (32) can be used for most isotropic linearly elastic material combinations if the initial maximum crack opening displacement is more than 10^{-5} of the crack radius.

For a single crack on an interface between two different solids we can introduce the normal, M_N, and transverse, M_T, elastic dissimilarity functions by normalizing the spring stiffness solutions of Eqs. (31) and (19) by that of Eqs. (32) and (20):

$$M_N(\alpha,\beta) = \frac{k^{0}_{N,dissimilar}}{k^{0}_{N,homogenous}} = \frac{(1+\alpha)\beta}{\pi\varepsilon(1+\varepsilon^2)(1-\beta^2)} \tag{34}$$

$$M_T(\alpha,\beta,\gamma) = \frac{k^{0}_{T,dissimilar}}{k^{0}_{T,homogenous}} = \frac{(1+\alpha)}{4(2-\upsilon_1)}\left(\frac{1}{\gamma}+\frac{4\beta}{\pi\varepsilon(1+\varepsilon^2)(1-\beta^2)}\right) \tag{35}$$

Fig. 6 shows M_N as contour plots as a function of α and β, varying from 0 (at $\alpha = -1$) to 2.355 (at $\alpha = 1$ and $\beta = 0.5$). Each circular symbol in Fig. 6 represents a material combination from Suga et al. (1988). Some commonly used material combinations are labeled with cross symbols. The M_N contours are nearly parallel to the β axis indicating that the α parameter is the dominant one in determining the value of M_N. The factor M_T in Eq. (35) depends not only on α and β but also on υ_1. The numerical value of M_T varies from zero (at $\alpha = -1$, G_2/G_1 approaches zero) to 2.177 (at $\alpha = 1$, G_2/G_1 approaches infinity and $\upsilon_1 = 0.5$).

By choosing $\upsilon_1 = 0.33$ ($\kappa_1 = 1.68$), M_T is plotted in the form of contour lines as a function of α and β in Fig. 7. Some material combinations with $\upsilon_1 = 0.33$ are labeled with cross-symbols. The limits of physically admissible material combinations are indicated by the lines of $\kappa_2 = 1$ and $\kappa_2 = 3$. As are the M_N contour lines in Fig. 6, the M_T contour lines in Fig. 7 are nearly parallel to the β-axis indicating that the α parameter is the dominant one in determining the value of M_T.

It has been shown (Lekesiz et al., 2011a) that the normal and tangential elastic dissimilarity function for a planar periodic array of collinear cracks at an interface between two dissimilar isotropic materials are identical and given in terms of Dundurs' parameters as

$$M^{2-D}(\alpha,\beta) = \frac{(1+\alpha)}{(1+4\varepsilon^2)(1-\beta^2)} \tag{36}$$

where the superscript, 2-D, is added to indicate strip cracks. Note that the form of M_N in Eq. (34) is somewhat similar to that for the 2D case, M^{2-D} in Eq. (36). In fact, Eq. (34) can be replaced by Eq. (36) with less than 0.8% maximum error for all material combinations. This indicates that the material dissimilarity function for the normal spring stiffness is nearly independent of the crack shape.

Using the solutions for the homogeneous case, Gorbatikh and Popova (2005) have shown that the common material parameter term $(1+\alpha)/(1-\beta^2)$ can be used to approximate the normal elastic compliances of non-interacting rectilinear, penny-shaped, elliptical and annular cracks at the interface between two dissimilar materials. Their independence of the crack shape (universal material parameter) is similar to our material dissimilarity factors, Eqs. (34) and (36), for the normal spring stiffness. Our argument above about comparison of 2D and 3D cases (Eqs. (34) and (36)) supports the notion of near independence of the normal elastic dissimilarity function of the crack shape. Eq. (34), however, provides an accurate expression for the material dissimilarity function specifically for a penny-shaped crack.

4.3. Spring stiffness for an array of penny-shaped cracks on dissimilar material interface

Eqs. (34) and (35) in Section 4.2 can be rewritten in slightly different manner:

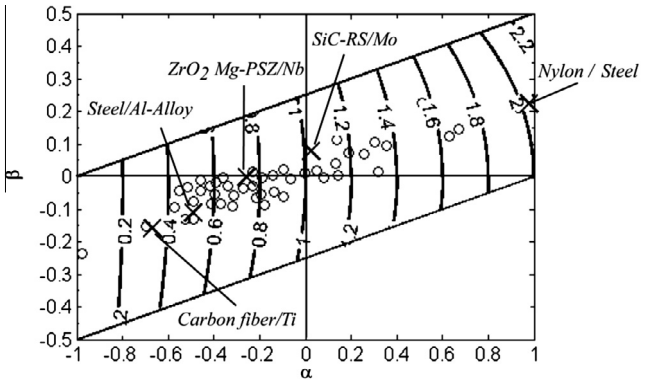

Fig. 6. Contour plots of the elastic dissimilarity function for the effective normal spring stiffness, M_N. Hollow circles (o) represent some material combination from Suga et al. (1988). Some material combinations are indicated by cross symbols (x) and labeled.

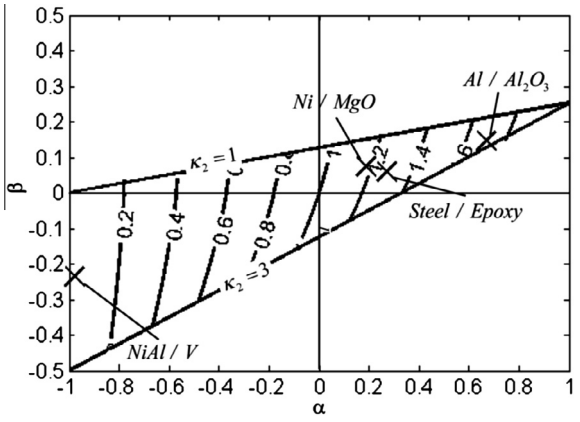

Fig. 7. Contour plots of the elastic dissimilarity function for the transverse spring stiffness, M_T, for $\upsilon_1 = 0.33$. Some sample material combinations with $\upsilon_1 = 0.33$ are indicated by cross symbols (x) and labeled.

$$k^0_{N,dissimilar} = M_N(\alpha,\beta) \times k^0_{N,\mathrm{hom}\,ogenous}$$
$$k^0_{T,dissimilar} = M_T(\alpha,\beta,\upsilon_1) \times k^0_{T,homogenous} \tag{37}$$

Combining them with Eqs. (30) leads to the approximate factorization of the effective stiffness for a periodic array of penny-shaped cracks at the interface between two dissimilar materials.

$$k^\infty_{N,dissimilar} \approx I^\infty\left(\frac{a}{b}\right) \times M_N(\alpha,\beta) \times k^0_{N,homogeneous} \tag{38}$$

$$k^\infty_{T,dissimilar} \approx I^\infty\left(\frac{a}{b}\right) \times M_T(\alpha,\beta,\upsilon_1) \times k^0_{T,homogeneous} \tag{39}$$

Inserting Eqs. 25, 34, 35 into Eqs. (38) and (39), we obtain the following explicit analytical expressions.

$$b\cdot k^\infty_{N,dissimilar} \approx \frac{E_1}{(1-\upsilon_1^2)}\frac{3\pi^3 C}{128}\frac{\beta(1+\alpha)}{\pi\varepsilon(1+\varepsilon^2)(1-\beta^2)} \times\sqrt{\frac{a}{b}}\left(\ln\left\{\sec\left[\frac{\pi}{2}\sqrt{C}\left(\frac{a}{b}\right)^{1.75}\right]\right\}\right)^{-1} \tag{40}$$

$$b\cdot k^\infty_{T,dissimilar} \approx \frac{E_1}{(1-\upsilon_1^2)}\frac{3\pi^3 C}{1024}(1+\alpha)\left(\frac{1}{\gamma}+\frac{4\beta}{\pi\varepsilon(1+\varepsilon^2)(1-\beta^2)}\right) \times\sqrt{\frac{a}{b}}\left(\ln\left\{\sec\left[\frac{\pi}{2}\sqrt{C}\left(\frac{a}{b}\right)^{1.75}\right]\right\}\right)^{-1} \tag{41}$$

In Eqs. (40) and (41), the effects of elastic dissimilarity, crack density and crack interaction on the effective spring stiffness are clearly represented. Recalling that $C = 0.8673$ and choosing four material combinations, BC4/Ni, Al_2O_3/Al Alloy, Steel/Al Alloy, Nylon/Steel, selected from Suga et al. (1988), Eqs (40) and (41) are respectively shown in Fig. 8(a) and (b). Since for low crack density ($a/b < 0.5$) the spring stiffness is nearly identical to that for the single crack, the range of the plot is chosen to be a/b larger than 0.5. As a/b increases, both the normal and transverse spring stiffness decreases for all material combinations. In general, transverse spring stiffness is observed to be smaller than normal spring stiffness.

4.4. Comparison of spring stiffness obtained in this work and those in literature

As discussed in Section 3, a distribution of effective spring stiffnesses, that substitute an array of coplanar interacting penny-shaped cracks in a homogeneous material, is a product of the spring stiffness for a non-interacting crack and the interaction function (Eq. (29)). Comparison of the interaction function ob-

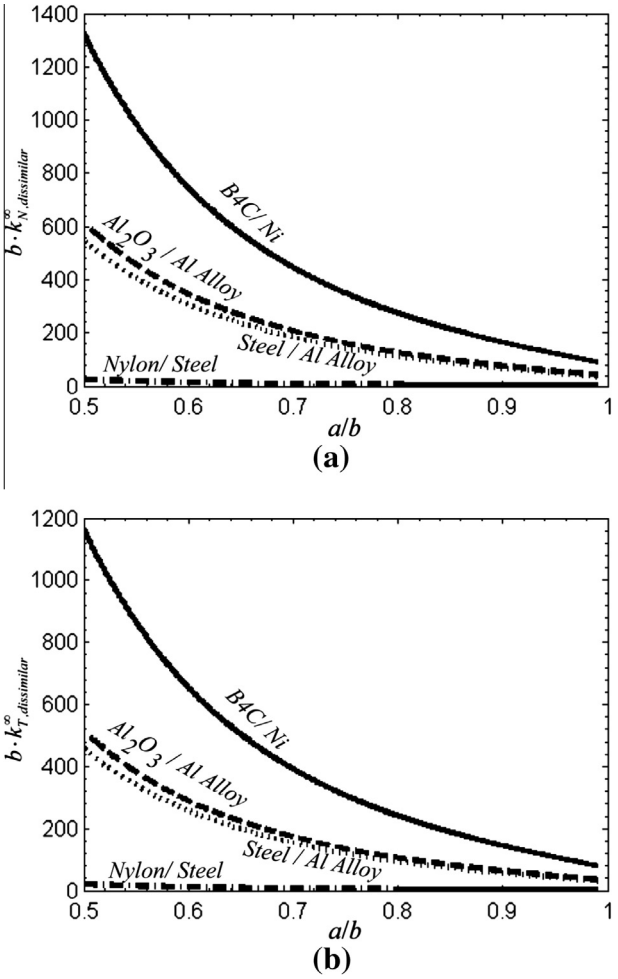

Fig. 8. Effective spring stiffness for four different material combinations with hexagonal array of penny-shaped interfacial cracks as a function of crack density parameter a/b (a) normal, (b) transverse.

tained in the current work and those available in the literature is given in Fig. 5(a) and (b).

For an array of coplanar interacting penny-shaped cracks at the interface between two dissimilar materials, the corresponding effective spring is in addition factored by the elastic dissimilarity function $M_{N,T}$, (Eqs. (38) and (39)). The normal and transverse spring stiffnesses versus a/b for a dissimilar material interface are compared with those models based on the literature in Fig. 9(a), using as an example of the steel-epoxy interface. As in Fig. 8, the range of a/b is chosen to be larger than 0.5 since for smaller a/b the spring stiffness becomes identical to that of non-interacting cracks studied by Lekesiz et al. (2011b). As in Fig. 8, transverse spring stiffness is smaller than normal spring stiffness and the spring stiffnesses obtained in this work are larger than those employed by Lavrentyev and Rokhlin (1994). Fig. 9(b) shows the total relative difference (in percent) as a function of a/b for the cases shown in Fig. 9(a) and the difference that is attributed to only material dissimilarity, without the crack interaction; it is independent of a/b; for small a/b those curves in Fig. 9(b) approach each other. Note that the results based on Lavrentyev and Rokhlin (1994) are for the square crack pattern while the current work is based on the hexagonal crack pattern.

Those results for the effective spring stiffness are surprisingly close in spite of various simplified assumptions in the Lavrentyev and Rokhlin (1994) model application to dissimilar materials: such as the use of an averaged Poisson's ratio and the well-known approximations for the aggregate Young's modulus in the punch

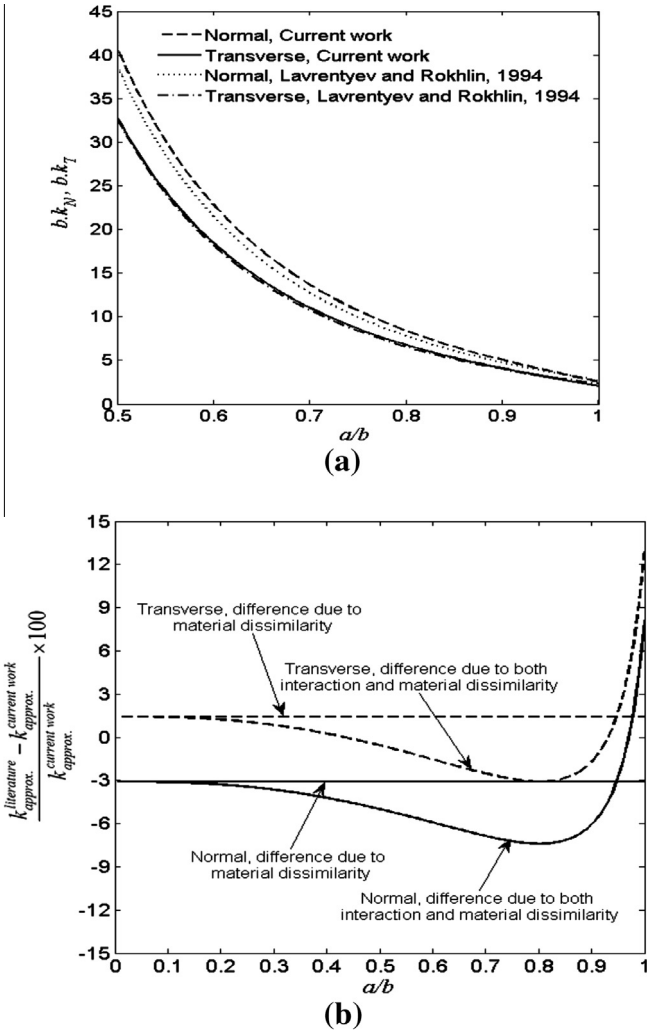

Fig. 9. Comparison of spring stiffness from the current work (hexagonal configuration) and that of Lavrentyev and Rokhlin, 1994 (square configuration): (a) normal and transverse spring stiffness (multiplied by half of the crack spacing, (b) for a periodic array of penny-shaped cracks at the steel/epoxy interface (E_{steel} = 215.3 - GPa ν_{steel} = 0.283, E_{epoxy} = 3.9 GPa ν_{epoxy} = 0.34); (b) relative difference (in percent) for the spring stiffness shown in (a).

model for dissimilar materials (see for example Johnson (1987)), that was used by Baik and Thompson (1984). Also Lavrentyev and Rokhlin (1994) have employed the original spring models by Baik and Thompson (1984) and Margetan et al. (1988) which have many model simplifications, while intuitively reasonable, are not based on rigorous analysis.

It is difficult to perform a direct estimate of a possible error that can be attributed to the assumptions and approximations made in the previous spring models for the cases considered in this work. Therefore, the conclusions from comparison with our results are important in validating the accuracy and applicability of the older models that have been used for experimental data analysis for a long time. However, our final results, Eqs. (40) and (41), which are obtained based on a rigorous analysis, are quite simple and can readily be used in place of previous phenomenological formulations.

5. Summary and conclusions

First, explicit expression of effective spring stiffness for a hexagonal array of coplanar penny-shaped crack in a homogeneous material is obtained using the strain energy which is evaluated through the stress intensity factors recently obtained by Lekesiz et al. (2013). Comparing this expression with the corresponding stiffness expression for non-interacting cracks in a homogeneous material, crack interaction for a hexagonal array of penny-shaped cracks as a function of crack density, a/b, is obtained. The crack interaction for the shear spring stiffness as a function of crack density and Poisson's ratio is shown to be identical to the crack interaction function for the normal spring stiffness, which is independent of Poisson's ratio.

Second, explicit expression of the material dissimilarity function is obtained based on the recently derived effective spring stiffness for non-interacting penny shaped cracks at the interface between two dissimilar materials (Lekesiz et al., 2011b). Lekesiz et al. (2011a) has recently shown that the effective spring stiffness for an array of 2D collinear cracks at the interface between two dissimilar materials can be represented approximately as a product of three factors: the material dissimilarity, the crack interaction function, and the effective spring stiffness for non-interacting cracks in a homogeneous material. In particular, the crack interaction factor for two dissimilar materials can be approximated by that for a homogeneous material for most practical material combinations.

Third, motivated by this 2D work and the fact that the crack interactions are generally weak in 3D compared to 2D, we propose simple explicit analytical expressions for the effective spring stiffness for an array of 3D penny-shaped cracks at the interface between two dissimilar materials factorizing it as the crack interaction function obtained for a homogeneous material and the material dissimilarity function obtained for non-interacting cracks at a dissimilar material interface.

The expressions obtained (for the hexagonal crack configuration) are shown to be close to the effective spring stiffness expressions based on intuitive assumptions (Lavrentyev and Rokhlin, 1994) for the square crack configuration. The current work, however, provides an approximate but rigorous formulation, which permits quick evaluation of the effect of material dissimilarity and crack density on the effective spring stiffness. And they can potentially be used to estimate interfacial micro-damage from experimental measurements of interfacial stiffness through ultrasonic methods, which is critical in estimating the remaining life of bonded structures.

Acknowledgements

The authors acknowledge partial support of this research by NIHDCR 1 R56DE021470-01 grant; SIR also acknowledges partial support by NASA NNX08BA37A Grant.

References

Angel, Y.C., Achenbach, J.D., 1985. Reflection and transmission of elastic-waves by a periodic array of cracks. J. Appl. Mech. Trans. ASME 52 (1), 33–41.
Baik, J., Thompson, R.B., 1984. Ultrasonic scattering from imperfect interfaces: a quasi-static model. J. Nondestruct. Eval. 4 (3/4), 177–196.
Baltazar, A., Wang, L., Xie, B., Rokhlin, S.I., 2003. Inverse ultrasonic determination of imperfect interfaces and bulk properties of a layer between two solids. J. Acoust. Soc. Am. 114, 1424–1434.
Benveniste, Y., 2006. A general interface model for a three-dimensional curved thin anisotropic interphase between two anisotropic media. J. Mech. Phys. Sol. 54, 708–734.
Buck, O., Thompson, R.B., Rehbein, D.K., Palmer, D.D., Brasche, L.J.H., 1989. Contacting surfaces: a problem in fatigue and diffusion bonding. Metall. Trans. A 20A, 627–636.
Delsanto, P.P., Scalerandi, M., 1998. A spring model for the simulation of the propagation of ultrasonic pulses through imperfect contact interfaces. J. Acoust. Soc. Am. 104 (5), 2584–2591.
Drinkwater, B.W., Dwyer-Joyce, R.C., Cawley, P., 1996. A study of the interaction between ultrasound and a partially contacting solid–solid interface. Proc. R. Soc. Lond. A 452, 2613–2628.
Dundurs, J., 1967. Effect of elastic constants on stress in a composite under plane deformation. J. Compos. Mater. 1, 310–322.

Dundurs, J., Bogy, D.B., 1969. Edge-bonded dissimilar orthogonal elastic wedges under normal and shear loading. J. Appl. Mech. 36 (3), 650–652.
Fabrikant, V.I., 1987. Close interaction of coplanar circular cracks in an elastic medium. Acta Mech. 67 (1–4), 39–59.
Fabrikant, V.I., 1989. Close interaction of coplanar circular cracks under shear loading. Comput. Mech. 4, 181–197.
Fabrikant, V.I., 1990. Complete solutions to some mixed boundary-value-problems in elasticity. Adv. Appl. Mech. 27, 153–223.
Gorbatikh, L., Popova, M., 2005. Estimation of elastic compliances of planar interfacial cracks from homogeneous solutions. Appl. Phys. Lett. 86 (3), 031905.
Hudson, J.A., Liu, E/., Crampin, S., 1997. The mean transmission properties of a fault with imperfect facial contact. Geophys. J. Int. 129 (3), 720–726.
Hutchinson, J.W., Suo, Z., 1992. Mixed mode cracking in layered materials. Adv. Appl. Mech. 29, 63–191.
Johnson, K.L., 1987. Contact Mechanics. Cambridge University Press, Cambridge, UK.
Kachanov, M., 1985. A Simple technique of stress-analysis in elastic solids with many cracks. Int. J. Fract. 28 (1), R11–R19.
Kachanov, M., 1987. Elastic solids with many cracks: a simple method of analysis. Int. J. Sol. Struct. 23 (1), 23–43.
Kachanov, M., 1994. Elastic solids with many cracks and related problems. Adv. Appl. Mech. 30, 259–445.
Kachanov, M., Laures, J.P., 1989. 3-Dimensional problems of strongly interacting arbitrarily located penny-shaped cracks. Int. J. Fract. 41 (4), 289–313.
Katoh, M., Nishio, K., Yamaguchi, T., 2002. Materials evaluation of diffusion bonded steel bar and its impact characteristics. NDE&E Int. 35, 263–271.
Lavrentyev, A.I., Rokhlin, S.I., 1994. Models for ultrasonic characterization of environmental degradation of interfaces in adhesive joints. J. Appl. Phys. 76 (8), 4643–4650.
Lavrentyev, A.I., Beals, J.T., 2000. Ultrasonic measurement of the diffusion bond strength. Ultrasonics 38, 513–516.
Lekesiz, H., Katsube, N., Rokhlin, S.I., Seghi, R.R., 2011a. Effective spring stiffness for a planar periodic array of collinear cracks at an interface between two dissimilar isotropic materials. Mech. Mater. 43, 87–98.
Lekesiz, H., Katsube, N., Rokhlin, S.I., Seghi, R.R., 2011b. Effective spring stiffness for non-interacting penny-shaped cracks at an interface between two dissimilar, isotropic, linearly elastic materials. Math. Mech. Sol. 7, 778–789.
Lekesiz, H., Katsube, N., Rokhlin, S.I., Seghi, R.R., 2013. The stress intensity factors for a periodic array of interacting coplanar penny-shaped cracks. Int. J. Sol. Struct. 50 (1), 186–200.
Liu, E., Hudson, J.A., Pointer, T., 2000. Equivalent medium representation of Fractured Rock. J. Geophys. Res. 105 (B2), 281–3000.
Margetan, F.J., Thompson, R.B., Gray, T.A., 1988. Interfacial spring model for ultrasonic interactions with imperfect interfaces: theory of oblique incidence and application to diffusion-bonded butt joints. J. Nondestruct. Eval. 7 (3/4), 131–152.
Margetan, F.J., Thompson, R.B., Rose, J.H., Gray, T.A., 1992. The interaction of ultrasound with imperfect interfaces: experimental studies of model structures. J. Nondestruct. Eval. 11 (3/4), 109–126.
Milne, K., Cawley, P., Nagy, P.B., Wright, D.C., Dunhill, A., 2011. Ultrasonic non-destructive evaluation of titanium diffusion bonds. J. Nondestruct. Eval. 30, 225–236.
Nagy, P.B., 1992. Ultrasonic classification of imperfect interfaces. J. Nondestruct. Eval. 11 (3/4), 127–139.
Palmer, D.D., Rehbein, D.K., Smith, J.F., Buck, O., 1988. Nondestructive Characterization of mechanical strength of diffusion bonds, II. Application of a quasi-static spring model. J. Nondestruct. Eval. 7 (3/4), 167–174.
Rice, J.R., 1988. Elastic fracture-mechanics concepts for interfacial cracks. J. Appl. Mech. Trans. ASME 55 (1), 98–103.
Rokhlin, S.I., Huang, W., 1993. Ultrasonic wave interaction with a thin anisotropic layer between two anisotropic solids. II: Second order asymptotic boundary conditions. J. Acoust. Soc. Am. 94, 3405–3420.
Rokhlin, S.I., Wang, Y.J., 1991. Analysis of boundary conditions for elastic wave interaction with an interface between two solids. J. Acoust. Soc. Am. 89, 503–515.
Rokhlin, S.I., Xie, B., Baltazar, A., 2004. Quantitative ultrasonic characterization of environmental degradation of adhesive bonds. J. Adhes. Sci. Technol. 18 (3), 327–359.
Roy, A., Chatterijee, M., 1994. Interaction between coplanar elliptic cracks. Normal loading. Int. J. Sol. Struct. 31 (1), 127–144.
Saha, T.K., Chatterjee, M., Roy, A., 1999. Interaction between coplanar elliptic cracks – II. Shear loading. Int. J. Sol. Struct. 36 (4), 619–637.
Sankar, T.S., Fabrikant, V.I., 1983. Punch and crack problems in transversely isotropic bodies. Int. J. Eng. Sci. 21 (7), 799–811.
Sih, G.C., 1973. Handbook of stress-intensity factors for researchers and engineers, in: Institute of Fracture and Solid Mechanics, Lehigh University.
Singher, L., Segal, Y., Segal, E., Shamir, J., 1994. Considerations in bond strength evaluation by ultrasonic guided waves. J. Acoust. Soc. Am. 96, 2497–2505.
Sotiropoulos, D.A., Achenbach, J.D., 1988. Ultrasonic reflection by a planar distribution of cracks. J. Nondestruct. Eval. 7 (3/4), 123–129.
Suga, T., Elssner, G., Schmauder, S., 1988. Composite parameters and mechanical compatibility of material joints. J. Compos. Mater. 22, 917–934.
Tada, H., Paris, P.C., Irwin, G.R., 2000. The Stress Analysis of Cracks Handbook. ASME Press, New York, NY.
Thompson, R.B., Thompson, D.O., 1991. Past experiences in the development of tests for adhesive bond strength. J. Adhes. Sci. Technol. 5 (8), 583–599.
Wang, Y., Katsube, N., Seghi, R.R., Rokhlin, S.I., 2007. Statistical failure analysis of adhesive resin cement bonded dental ceramics. Eng. Fract. Mech. 74, 1838–1856.
Wang, W., Rokhlin, S.I., 1991. Evaluation of interfacial properties in adhesive joints of aluminum-alloys using angle-beam ultrasonic spectroscopy. J. Adhes. Sci. Technol. 5 (8), 647–666.
Willis, J.R., 1972. Penny-shaped crack on an interface. Q. J. Mech. Appl. Math. 25, 367–385.